Effect of Honeycomb Porous Plate on Critical Heat Flux in Saturated Pool Boiling of Artificial Seawater

Wilton Fogaça[1], Shoji Mori[2*], Kousuke Imanishi [2], Kunito Okuyama[2], J.R.C. Piqueira[1]

[1] *School of Engineering*

University of São Paulo

Av. Prof. Luciano Gualberto, 380 - Butantã, São Paulo - SP, Brazil

[2] *Department of Chemical Engineering Science*

Yokohama National University

79-5 Tokiwadai, Hodogaya, Yokohama, Japan

*Shoji Mori
Address: 79-5 Tokiwadai, Hodogaya, Yokohama, Japan
Email address: morisho@ynu.ac.jp (Shoji Mori)
Tel: 81-45-339-4010

Abstract

During a severe nuclear power plant accident, the integrity of the reactor pressure vessel must be assured. In response to a possible fuel meltdown, operators of the current generation of nuclear power plants are likely to inject water into the reactor pressure vessel to cool down the reactor vessel wall, preserving its integrity and avoiding leakage of radioactive material. This study considers the use of seawater to flood a reactor pressure vessel combined with the attachment of a honeycomb porous plate (HPP) on the vessel outer wall as a way to improve the safety margins for in-vessel retention of fuel. In long-duration experiments, saturated pool boiling of artificial seawater was performed with an upward-facing plain copper heated surface 30 mm in diameter. The resulting value for critical heat flux (CHF) was 1.6 MW/m^2 at atmospheric pressure, a value significantly higher than the CHF obtained when the working fluid was distilled water (1.0 MW/m^2). It was verified that sea-salt deposits could greatly improve surface wettability and capillarity, enhancing the CHF. The combination of artificial seawater and an HPP attached to the heated surface improved the boiling heat transfer coefficient and increased the CHF up to 110% (2.1 MW/m^2) as compared to distilled water on a bare surface. After the artificial seawater experiments, most of the wall micropores of the HPP were clogged because of sea-salt aggregation on the HPP top and bottom surfaces. Thus, the CHF enhancement observed in this case was attributed mainly to the separation of liquid and vapor phases provided by the HPP channel structure and improvement of surface wettability and capillarity by sea-salt deposition.

Keywords:

Saturated pool boiling, In-vessel retention, Seawater cooling, Critical heat flux, Honeycomb porous plate, Sea-salt deposition

Nomenclature

q	heat flux (W/m^2)
h	boiling heat transfer coefficient (W/(m^2·K))
T	temperature (K)
d_1	diameter of heat transfer surface (m)
d_2	diameter of copper block upper body (m)
d_{ch}	honeycomb porous plate channel width (m)
k	thermal conductivity (W/(m·K))
c_{pl}	specific heat of liquid (J/(kg·K))
H_{lg}	latent heat of evaporation (J/kg)
C_{sf}	Rohsenow correlation constant
g	gravitational acceleration (m/s^2)

Greek characters

δ_h	height of the honeycomb porous plate (m)
δ_w	width of the honeycomb porous plate wall (m)
ρ	density (kg/m^3)

μ	viscosity (N·s/m^2)
σ	surface tension (N/m)

Subscripts

l	liquid
v	vapor
w	wall
i	thermocouple number
sat	saturation
CHF	critical heat flux

1. Introduction

Increasing safety is vital for the future of nuclear power plants, so great effort has been invested in making accident management techniques more reliable for the next generation of nuclear reactors [1]. A potential scenario for severe nuclear accidents is reactor core meltdown, during which core debris relocates to the lower head of the reactor pressure vessel (RPV) and threatens its integrity. In-vessel retention (IVR) is a set of strategies that aims to confine this debris and control RPV damage. Next-generation nuclear reactors are built to allow flooding of the vessel cavity with water to remove core decay heat through the external wall of the RPV, avoiding its structural failure and release of radioactive material.

Various methods have been proposed for enhancing IVR performance and reliability, including using nanofluids [2–5] or surfactant solutions [6–8] instead of water and modifying the RPV outer wall [9–14]. Mori et al. [15] proposed a combination of two approaches, the adoption of TiO_2 nanofluid as coolant and the attachment of a honeycomb porous plate (HPP) to the RPV outer wall to improve the critical heat flux (CHF). They found that the CHF increased when using the nanofluid concentrations tested (0 vol%, 0.001 vol%, and 0.1 vol%), with a CHF of 3.2 MW/m^2 for 0.1 vol% nanofluid with an HPP attached to the surface. This CHF was more than three times the CHF of pure water on the same surface without the HPP (1.0 MW/m^2).

Due to a shortage of freshwater, seawater was employed during the 2011 accident at the Fukushima Daiichi Nuclear Power Plant. This event raised the question of whether seawater can be employed as coolant during IVR efforts. If its viability is proven, seawater could represent a simple and economically attractive alternative compared with other methods.

Raghupathi and Kandlikar [16] investigated artificial seawater pool boiling on a 10 mm x 10 mm copper boiling surface and compared the results to those for distilled water. They found the CHF of seawater to be 52% higher than that of distilled water. They also studied the effect of scale formation during extended periods of time at an approximately constant heat flux. To this end, they developed a passive method using stainless steel beads to remove scale from the boiling surface during the experiment. Without the beads, the wall superheat increased from 27 K to 34 K during the boiling experiment. Adding the beads resulted in significantly lower wall superheat, which decreased from 16.6 K at the beginning of the experiment to 12.0 K at the end. From these experiments, they concluded that additional nucleation sites and increased thermal resistance due to scale formation were responsible for the higher CHF and wall superheat observed for artificial seawater.

Uesawa et al. [17] performed experiments for nucleate pool boiling of distilled water, solutions of NaCl (3.5 wt%, 7 wt%, and 10 wt%), artificial seawater (3.5 wt%, 7 wt%, and 10 wt%), and real seawater on a 10 mm x 10 mm copper printed circuit board surface. Similar CHF values were found for distilled water (0.92 MW/m^2), NaCl solutions (0.95 MW/m^2), real seawater (0.95 MW/m^2), and artificial seawater with a concentration of 3.5 wt% (0.96 MW/m^2). The accumulation of deposits was only observed for artificial seawater with concentrations of 7 wt% and 10 wt%, which produced CHFs of 0.60 MW/m^2 and 0.12 MW/m^2, respectively. Moreover, the layer of salt deposited during the experiment on the boiling surface was verified to be mainly composed of $CaSO_4$.

The present study focused on clarifying the effect of a HPP on the CHF in saturated pool boiling of seawater, which represents the first step toward investigating whether IVR can be improved by combining an HPP attached to the outer wall of the RPV with the use of seawater to flood the

vessel cavity. If feasible, both options are economically attractive and easily applied in comparison with other IVR alternatives.

2. Experimental apparatus and procedures

2.1. Experimental apparatus

Figure 1 is a schematic of the experimental apparatus, which was housed in a cylindrical Pyrex glass vessel with a height of 500 mm and inner diameter of 87 mm. The apparatus has a condenser to keep the working fluid volume constant, a pre-heating element of 25 Ω resistance to degas the working fluid, and a K-type thermocouple to monitor the fluid bulk temperature.

< Figure 1 >

The boiling surface was a circular upward-facing plain copper surface of 30 mm in diameter. It was the top of a copper block which had seven cartridge heaters (13.7 Ω) at the bottom. Except for boiling surface which is referred to heated surface in the following, the copper block was covered with fiberglass insulation to avoid heat losses as much as possible. The upper part of the copper block body was a cylinder 32 mm in diameter, and it had four thermocouples (TC1, TC2, TC3, and TC4), spaced 5 mm apart and inserted in its central axis. Figure 1 also shows a detailed sketch of the copper block. Outputs from TCs were recorded at a sample frequency of 1 Hz during the experiment.

2.2. Honeycomb porous plate

The HPP used in this experiment was a ceramic grid structure, made of *$CaOAl_2O_3$ (30-50 wt%), fused SiO_2 (40-60 wt%) and TiO_2 (5-20 wt%),* with 200 cells/inch^2. Figure 2 shows the structural design and dimensions of the HPP. Its porous walls had a height δ_h of 1 mm and thickness $\delta_w$of 0.4 mm; the walls had capillary pores with a median radius of 0.13 μm and porosity of 24.8% and square-shaped channels (cells) with side width $d_{ch}$of 1.3 mm. These channels provided a path for vapor to leave the heated surface.

The CHF enhancement capability of an HPP lies in two main mechanisms: (1) the capillary action provided by the micropores in its walls, which draws the fluid toward the boiling surface, and (2) the separation of fluid and vapor flow paths in the channels. The vapor leaves the heated surface at the center of the channels and the liquid is pulled toward the surface by gravity at the channel edges. The performance and CHF enhancement capabilities of the HPP employed here were extensively studied by Mori et al. [18,19].

< Figure 2 >

No adhesive was employed to fix the HPP to the surface; instead, it was attached by pressing it against the surface with stainless steel wires. Figure 3 shows the boiling surface with and without the HPP installed.

< Figure 3 >

2.3. Working fluid

The artificial seawater was prepared by adding 35 g of Red Sea Salt from Red Sea Aquatics, Ltd., to 1 L of distilled water. The resulting artificial seawater had a concentration of salts and composition close to the average values found in real seawater [20], as shown by the elemental comparison presented in Table 1.

< Table 1 >

2.4. Experimental procedures

To prepare the boiling surface, it was polished with 2,000-grit abrasive paper and cleaned with acetone. The vessel was filled with working fluid to a level 60 mm above the boiling surface. The working fluid was heated and maintained at its saturation temperature for 40 min to degas it. The pre-heater used to degas the water had a surface area of 0.014 m^2 and resistance of 25.0 Ω. A voltage of 100 V was applied to it, which resulted in a heat flux of 0.03 MW/m^2 during degasification. According to the analysis result Electron Probe Micro Analyze (EPMA), formation of $CaCO_3$ may initiate at this stage of pre-heating although the heat flux is extremely small. All experiments were conducted at atmospheric pressure.

The heat flux was raised from 0 to the CHF value in steps of approximately 0.1 MW/m^2. The CHF was adopted as the last stable heat flux. At each step, the voltage in the cartridge heaters was kept constant until a quasi-steady-state was achieved, which was defined as a state in which the temperature did not change more than 0.25 K for at least 10 min.

With the system at quasi-steady-state condition, the linearity of temperature distribution in the copper block was checked carefully and then the wall temperature and heat flux were calculated using Fourier's Law. The thermal conductivity of the copper was evaluated using the arithmetic mean of the measured temperatures in the considered region.

For each quasi-steady-state condition, three values for heat flux, surface temperature, and heat transfer coefficient were obtained by combining the temperatures of two non-consecutive thermocouples. The chosen thermocouple pairs for the calculations were TC1-TC3, TC1-TC4, and TC2-TC4. At each step, the average of these values was recorded as a final value. The experiments to obtain boiling curves, with minimum duration of 5 h, were repeated three times in each case. The results shown are average results from all the experiments. The standard deviation for the CHF was lower than 0.05 MW/m^2 for every case studied, indicating a good reproducibility of the experiments.

The uncertainty analysis was performed using the standard deviation and the propagation of uncertainty [21], calculated as follows:

$$\sigma_f = \sqrt{\sum_{i=1}^{N} \left[\left(\frac{\partial f}{\partial x_i} \right) \sigma_{x_i} \right]^2} \quad (1)$$

where $f(x_1, x_2, \ldots, x_N)$ is the function for which uncertainty is desired and σ_{x_i} is the uncertainty of the i-th variable.

In order to verify heat flux distribution through the heated surface, two additional thermocouples were installed on the side surface of the copper block. As a result, heat flux distribution was small, that is, the difference of heat flux at the center and outer part of the surface was up to 0.1 MW/m^2 for *approximately 2.0 MW/m^2*.

The uncertainty of the heat fluxes, BHTCs and excess of temperature, for values of heat flux equal or higher than 1.0 MW/m^2, were approximately 7%, 10% and 7% of the measured value, respectively.

3. Results and discussion

The first step toward investigating artificial seawater pool boiling with an HPP was to determine whether sea-salt deposition on the boiling surface could reduce the BHTC, making the wall temperature continuously increase and triggering a transition to film boiling.

Accordingly, long-duration pool boiling tests were conducted with and without the HPP. The temperature of the surface was monitored for 11 h at a heat flux of approximately 1.0 MW/m^2. The results are shown in Figure 4. To begin these experiments, the heat flux was suddenly raised from 0 to 1.0 MW/m^2, and the first measurement was taken after 30 min, which is also the time interval between each data point in the figure. An experiment with distilled water on the bare surface (BS) for 3 h was also conducted for comparison.

< Figure 4 >

Boiling of artificial seawater achieves a quasi-steady-state as defined in section 2.4 could be achieved. For the case of BS and artificial seawater, it took 2.5 h to reach the quasi-steady-state due to the formation of a salt layer on the BS. During this interval, the salt layer thickened gradually on the surface until it finally reached quasi-equilibrium-state.

When the HPP was attached, the time required to reach the quasi-steady-state decreased to 1.5 h, and the temperature of the surface, after 11 hours of experiment was 7 K lower when compared to BS case due to improvement of the BHTC provided by the HPP [18,19]. Since the temperature increases with the same rate during transient in BS and HPP, the lower temperature at quasi-steady-state resulted in a shorter transient time.

Figure 5 compares the surface deposits after 5 hours of seawater pool boiling with and without the HPP. The presence of white crystals with thickness distribution on the heated surface could be observed in both cases.

< Figure 5 >

Figure 5(a) shows that the surface was entirely covered with a sea-salts layer after artificial seawater pool boiling without the HPP. With the HPP, shown in Figure 5(b), sea-salt deposits presented a non-uniform concentration of deposits along the surface.

The salt deposits formed in the case with the HPP was analyzed using a 3D laser scanning confocal microscope (VK-X250, Keyence) with measurement accuracy of 0.2 μm. 4 different measurement area (approximately 1.5 mm x 1.5 mm) was examined.

Figures 6 indicate (a) optical images, (b) height profiles and (c) the sectional view of the dashed line in (b) of typical deposit configuration at channels, wall intersections and wall positions, respectively. The height of deposits in every channel was similar with average height of 13.3(±0.8) μm. Deposits formed under wall intersections and wall positions show a wide variety of heights along the surface. Heights ranging from 20 μm to 50 μm (averaged value: 29.6±10.5 μm)were found at wall intersection and from 10 μm to 30 μm(averaged value: 21.1±7.8 μm) at wall positions.

Electron Probe Micro Analyze (EPMA) measurements of the sea-salts deposits revealed that, for the experiments presented here, its primary composition was NaCl. Table 2 shows the atomic ratio of the main elements found in the deposits.

< Table 2 >

< Figure 6 >

After experiments with the HPP, it was noticed that the color of the outer parts of the copper surface slightly changed due to oxidation. However, the oxide layer thickness has an order of magnitude of nanometers [22] and its effect on CHF and BHTC was judged to be negligible under the conditions considered here. Therefore, it is assumed that sea salt constituted the vast majority of material that adhered to the heated surface during the experiments.

The long-duration experiments showed that salt layer growth strongly depends on time, so long-duration pool boiling experiments are important for understanding the changes in the boiling surface and conditions.

Next, additional artificial seawater CHF experiments were performed to examine the influence of the HPP on the CHF in detail. **Figure 7** condenses the results of distilled water and artificial seawater on the BS and on the surface with the HPP. The open and closed symbols represent the CHF and the BHTC, respectively. The percentage values alongside the arrows indicate the enhancement obtained relative to distilled water on the BS.

< Figure 7 >

The CHF of artificial seawater on the BS (◇) was 1.6 MW/m^2, a value 60% higher than that found for distilled water (○), which was 1.0 MW/m^2. This result is similar to that of Raghupathi and Kandlikar [16], who found a 52% improvement for the CHF of artificial seawater when compared to distilled water.

To verify changes in surface properties due to the deposited salt layer, a wettability test was performed before and after the artificial seawater pool boiling. In this test, a drop of water of approximately 1 μL was placed on the surface and the spreading of the wetted area was recorded with a high-speed camera at 1,000 frames per second. The tests were performed at room temperature without an environmental control enclosure.

Although it was not possible to assure exactly the same experimental conditions for every run, the purpose of the test was to provide qualitative information about the surface with and without the sea-salt layer. Furthermore, the effect of salts dissolution in the droplet of distilled water

during this experiment was checked through the replacement of it by saturated seawater solution, which corresponds to sea-salts solution with concentration of approximately 350 g/l (26 wt%) at room temperature. This verification revealed that, for the qualitative analysis proposed here, the effect of salts dissolution in the wetted area is not significantly.

Figure 8 shows images of the spreading wetted area for four recording times; these and the other images were used to approximate the area circumferences. The first image on the left (0 ms) depicts the moment the droplet touched the surface. The wetted area spreading as a function of time for the first 160 ms is presented in **Figure 9**.

The wetted area spread faster on the surface with salt deposits, and it became significantly wider in comparison to the wetted area on the clean surface. This supports the hypothesis that sea-salt deposition can improve wettability and capillarity of the boiling surface. These results are consistent with the higher CHF observed for artificial seawater.

< Figure 8 >

< Figure 9 >

As shown in **Figure 7**, attachment of the HPP enhanced the CHF in all cases when compared to the BS experiments. The CHFs for distilled water (□) and artificial seawater (△) with the HPP were both 2.1 MW/m^2. For the case with an HPP in distilled water the HPP capillary action, which continuously draws bulk liquid toward the heated surface, and the separation of liquid and vapor paths mitigates competition for space between the two phases near the surface, thereby increasing the CHF.

The BHTCs for both fluids were also improved with the HPP. Nevertheless, in both cases, artificial seawater presented a lower BHTC in comparison to distilled water. This showed that sea-salt deposition may jeopardize the BHTC. The main component of the deposit layer, NaCl, has a relatively low thermal conductivity (4.9 W/m·K) [23]; This thermal resistance due to deposit layer could lead to the lower BHTC observed in the artificial seawater experiments.

Figure 10 shows the boiling curves and BHTCs for all the cases studied here. Predicted boiling curves obtained from the Rohsenow correlation [24] using the properties of distilled water and seawater are shown in this figure as dashed lines. The Rohsenow formula is

$$\frac{c_{pl}}{H_{lg}}\Delta T_{sat} = C_{sf}\left[\frac{q}{\mu_l H_{lg}}\sqrt{\frac{\sigma}{g(\rho_l-\rho_v)}}\right]^{0.33}\left(\frac{c_{pl}\mu_l}{k_l}\right)^{1.7} \quad (2)$$

where c_{pl} is the specific heat of liquid; H_{lg} is the latent heat of evaporation; μ_l is the viscosity of liquid; g is gravitational acceleration; σ is the surface tension; k_l is the thermal conductivity of liquid; ρ_v and ρ_l are the density of vapor and liquid, respectively; and $C_{sf} = 0.013$ is the constant adopted in both cases. The physical properties of seawater at its saturation temperature were obtained from Nayar et al. [25] and Sharqawy et al. [26].

< Figure 10 >

The boiling curve of distilled water (○) is in good agreement with the Rohsenow's correlation. The curve for artificial seawater (◇) diverges to the right of the distilled water curve after approximately 0.5 MW/m^2. Although it was verified that deposition started in the early stages of the experiments, this comparison suggests that the effects of additional thermal resistance

becomes prominent for pool boiling performance after the heat flux reaches 0.5 MW/m^2. As expected, for higher heat fluxes the additional thermal resistance resulted in a larger superheat in the artificial seawater curves. The surface superheat, as indicated by the CHF condition, for artificial seawater on the BS (◇) (31.9 K) was relatively high when compared to distilled water (○) (19.2 K).

Scanning electron microscope (SEM) images of the copper surface and HPP before and after the pool boiling experiment with artificial seawater are shown in **Figure 11**. The HPP surfaces shown are the top and bottom of a wall intersection.

Comparison of the boiling surface images shows that sea-salt deposits largely increased the surface's roughness, which contributed to improved CHF [27]. Before the experiments, the HPP had irregular top and bottom wall intersection surfaces with relatively sharp shapes. The images after the experiment show that sea salt filled in the spaces on the HPP surfaces. The appearance of sea-salt on top of the HPP surfaces was attributed to two sources: (1) The formation of $CaCO_3$ from pre-heating; (2) the generation of salt layer fragments from the boiling surface during the experiment. Bubbles leaving the boiling surface suspend sea-salt particles and fragments and carry them into the bulk liquid, and later they accumulate on the top of the HPP surfaces.

< Figure 11 >

To verify potential pore blockage by the sea salt, pool boiling experiments were performed with both working fluids using three HPPs with different pore conditions: a brand-new HPP, designated new HPP (NHPP); an HPP used in artificial seawater experiments, designated

deposited HPP (DHPP); and an HPP with no pores, designated honeycomb solid plate (HSP). The HSP was obtained by covering the porous walls of an HPP with silicone adhesive to completely suppress the capillary action.

Figure 12 presents the boiling curves for distilled water on the BS and with the NHPP and HSP. When the HSP was used, the CHF was 1.2 MW/m^2, which is considerably lower than the CHF with the NHPP (2.1 MW/m^2). From these results, two main conclusions can be made for distilled water case: (1) the capillary action of the HPP is responsible for more than 80% of the CHF enhancement and thus is the most important mechanism and (2) the grid design of the HPP contributes to CHF improvement.

< Figure 12 >

< Figure 13 >

Figure 13 presents the boiling curves for artificial seawater with all three HPP pore conditions (NHPP, DHPP, and HSP). Due to experimental accuracy, it is not possible to distinguish the results for NHPP or DHPP with artificial seawater. Repetitive use of the same DHPP did not provide any perceptible change in the CHF value, BHTC, or boiling curve behavior. These findings suggest that the blockage of pores reached a saturation point during their first exposure to artificial seawater.

Furthermore, within the accuracy of the experimental apparatus, the difference between the CHFs of the NHPP/DHPP and HSP was not significantly. This leads to the conclusion that capillarity makes only a small contribution to CHF improvement. Thus, the most important mechanisms of CHF improvement are the separation of liquid and vapor paths provided by the

grid design of the HPP structure and the sea salt layer formed on the copper surface. Moreover, the difference in CHF values when the HSP was used in distilled water and artificial seawater can be attributed to the sea-salt deposits.

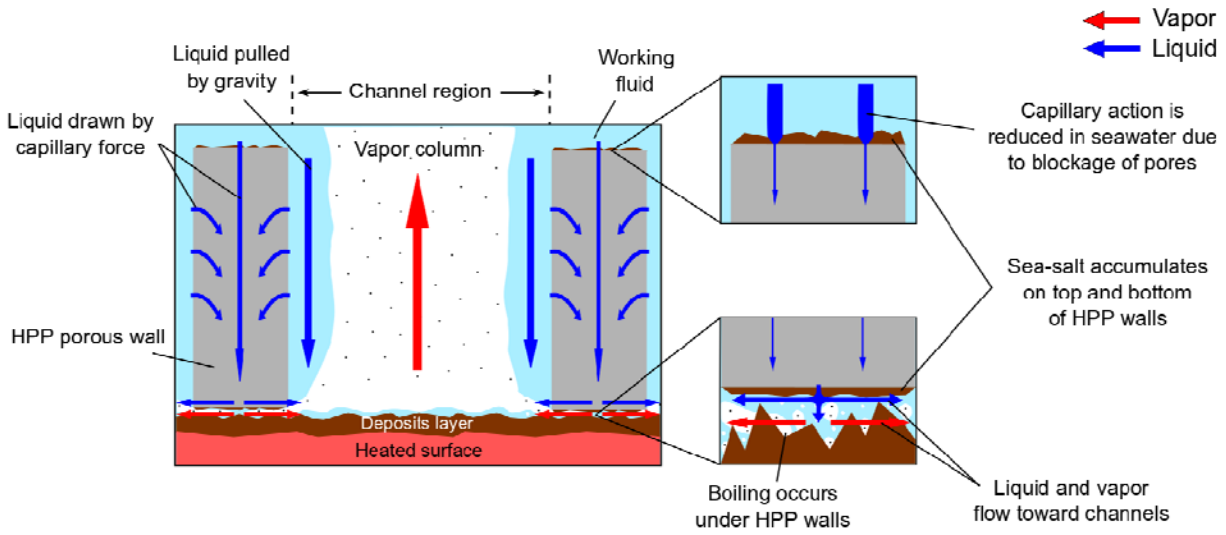

Figure **14** summarizes the main characteristics of pool boiling of artificial seawater with an HPP installed. The most important points are:

- Boiling occurs predominantly at channel positions, where intense deposition is observed,
- Sea salt accumulates on the HPP top and bottom surfaces, reducing the permeability of an HPP, and
- Supply of liquid by the gravity force through the channels and the deposited layer are the main mechanisms responsible for CHF enhancement.

< Figure 14 >

Although the obtained results suggest the combination of artificial seawater and an HPP could equal or surpass the CHF of distilled water in pool boiling, which is an important parameter for

IVR safety, further investigations are needed to determine its effectiveness in a real accident situation. A wider variety of scenarios as different inclination angles of the heater surface, higher system pressure, denser concentrations of salt and flow boiling regime still need to be addressed. A deep examination of the deposits and its effects on boiling performance and on the HPP in these conditions is also required in order to determine the viability of seawater as coolant.

4. Conclusion

The heat transfer performance of artificial seawater in pool boiling with and without the attachment of an HPP to the heated surface was investigated and compared to that of pool boiling with distilled water. The conclusions are as follows:

(1) On the BS, the CHF of artificial seawater was 1.6 MW/m^2, which is 60% higher than that of distilled water. The CHF improvement was attributed to the surface wettability and capillarity enhancement due to the deposition of sea-salt during boiling. The salt layer also increased the thermal resistance of the surface, resulting in a higher surface superheat.

(2) Attachment of an HPP to the heated surface was shown to be an effective strategy for enhancing both the CHF and BHTC. In the case of artificial seawater, the CHF improved to 2.1 MW/m^2. When compared to distilled water on the BS, this represents a 110% improvement.

(3) Blockage of most of the HPP micropores by sea salt was observed during pool boiling of artificial seawater, indicating that capillary action has a minor role in CHF enhancement for seawater. Instead, the main contribution comes from the separation of liquid and vapor phases near the boiling surface provided by the HPP channel structure and the improvement of surface wettability provided by salt deposition. This is different from what was observed for distilled water, where the capillary action was the most important mechanism of CHF enhancement.

5. Acknowledgments

All the experiments were conducted at the Department of Chemical Engineering Science of Yokohama National University. This work was partially supported by Coordination for the Improvement of Higher Education Personnel and JSPS Kakenhi Grant Number 15H03928.

6. References

[1] W. Ma, Y. Yuan, B.R. Sehgal, In-Vessel Melt Retention of Pressurized Water Reactors: Historical Review and Future Research Needs, Engineering. 2 (2016) 103–111. doi:10.1016/J.ENG.2016.01.019.

[2] J. Buongiorno, L.W. Hu, G. Apostolakis, R. Hannink, T. Lucas, A. Chupin, A feasibility assessment of the use of nanofluids to enhance the in-vessel retention capability in light-water reactors, Nucl. Eng. Des. 239 (2009) 941–948.

doi:10.1016/j.nucengdes.2008.06.017.

[3] Q.T. Pham, T.I. Kim, S.S. Lee, S.H. Chang, Enhancement of critical heat flux using nano-fluids for Invessel Retention-External Vessel Cooling, Appl. Therm. Eng. 35 (2012) 157–165. doi:10.1016/j.applthermaleng.2011.10.017.

[4] S.D. Park, I.C. Bang, Flow boiling CHF enhancement in an external reactor vessel cooling (ERVC) channel using graphene oxide nanofluid, Nucl. Eng. Des. 265 (2013) 310–318. doi:10.1016/j.nucengdes.2013.08.064.

[5] G. Dewitt, T. McKrell, J. Buongiorno, L.W. Hu, R.J. Park, Experimental study of critical heat flux with alumina-water nanofluids in downward-facing channels for In-Vessel Retention applications, Nucl. Eng. Technol. 45 (2013) 335–346. doi:10.5516/NET.02.2012.075.

[6] Y.H. Jeong, M.S. Sarwar, S.H. Chang, Flow boiling CHF enhancement with surfactant solutions under atmospheric pressure, Int. J. Heat Mass Transf. 51 (2008) 1913–1919. doi:10.1016/j.ijheatmasstransfer.2007.06.044.

[7] T. Il Kim, H.M. Park, S.H. Chang, CHF experiments using a 2-D curved test section with additives for IVR-ERVC strategy, Nucl. Eng. Des. 243 (2012) 272–278. doi:10.1016/j.nucengdes.2011.11.031.

[8] J. Lee, Y.H. Jeong, S.H. Chang, CHF enhancement in flow boiling system with TSP and boric acid solutions under atmospheric pressure, Nucl. Eng. Des. 240 (2010) 3594–3600. doi:10.1016/j.nucengdes.2010.05.027.

[9] Y.H. Jeong, W.J. Chang, S.H. Chang, Wettability of heated surfaces under pool boiling using surfactant solutions and nano-fluids, Int. J. Heat Mass Transf. 51 (2008) 3025–3031. doi:10.1016/j.ijheatmasstransfer.2007.09.023.

[10] J. Yang, M.B. Dizon, F.B. Cheung, J.L. Rempe, K.Y. Suh, S.B. Kim, CHF enhancement by vessel coating for external reactor vessel cooling, Nucl. Eng. Des. 236 (2006) 1089–1098. doi:10.1016/j.nucengdes.2005.11.008.

[11] F.A. Sohag, F.R. Beck, L. Mohanta, F.B. Cheung, A.E. Segall, T.J. Eden, J.K. Potter, Enhancement of Downward-Facing Saturated Boiling Heat Transfer by the Cold Spray Technique, Nucl. Eng. Technol. 49 (2017) 113–122. doi:10.1016/j.net.2016.08.005.

[12] F. Hou, H. Chang, Y. Zhao, M. Zhang, T. Gao, P. Chen, Experimental study of critical heat flux enhancement with hypervapotron structure under natural circulation conditions, Nucl. Eng. Des. 316 (2017) 209–217. doi:10.1016/j.nucengdes.2017.03.013.

[13] S. Mori, S. Mt Aznam, K. Okuyama, Enhancement of the critical heat flux in saturated pool boiling of water by nanoparticle-coating and a honeycomb porous plate, Int. J. Heat Mass Transf. 80 (2015) 1–6. doi:10.1016/j.ijheatmasstransfer.2014.08.046.

[14] S. Mt Aznam, S. Mori, F. Sakakibara, K. Okuyama, Effects of heater orientation on critical heat flux for nanoparticle-deposited surface with honeycomb porous plate attachment in saturated pool boiling of water, Int. J. Heat Mass Transf. 102 (2016) 1345–1355. doi:10.1016/j.ijheatmasstransfer.2016.07.004.

[15] S. Mori, S. Mt Aznam, R. Yanagisawa, K. Okuyama, CHF enhancement by honeycomb porous plate in saturated pool boiling of nanofluid, J. Nucl. Sci. Technol. 53 (2016) 1028–1035. doi:10.1080/00223131.2015.1087353.

[16] S.G. Raghupathi, Pruthvik A. and Kandlikar, Preliminary results of pool boiling of seawater, 14th Int. Conf. Nanochannels, Microchannels, Minichannels. (2016). doi:10.1115/ICNMM2016-7972.

[17] S. Uesawa, Y. Koizumi, M. Shibata, H. Yoshida, Pool Nucleate Boiling on Heat Transfer

Surface With Deposited Sea Salts, ICONE24. (2016) 1–16.

[18] S. Mori, L. Shen, K. Okuyama, Effect of Cell Size of a Honeycomb Porous Plate Attached to a Heated Surface on CHF in Saturated Pool Boiling, 14th Int. Heat Transf. Conf. (2011) 1–11.

[19] S. Mori, K. Okuyama, Enhancement of the critical heat flux in saturated pool boiling using honeycomb porous media, Int. J. Multiph. Flow. 35 (2009) 946–951. doi:10.1016/j.ijmultiphaseflow.2009.05.003.

[20] F.J. Millero, R. Feistel, D.G. Wright, T.J. McDougall, The composition of Standard Seawater and the definition of the Reference-Composition Salinity Scale, Deep Sea Res. Part I Oceanogr. Res. Pap. 55 (2008) 50–72. doi:10.1016/j.dsr.2007.10.001.

[21] B.N. Taylor, C.E. Kuyatt, Guidelines for Evaluating and Expressing the Uncertainty of NIST Measurement Results, NIST Tech. Note. 1297 (1994) 20.

[22] M. Moliere, Y. Verdier, C. Leymonie, Oxidation of copper in high purity water at 70°C: Application to electric generator operation, Corros. Sci. 30 (1990) 183–188. doi:10.1016/0010-938X(90)90072-D.

[23] P.E. Ohlsen, Thermal conductivity of sodium chloride within the temperature range 375 K to 637 K.pdf, (1956). http://scholarsmine.mst.edu/masters_theses/2573.

[24] A. Rohsenow, A Method of Correlating Heat Transfer Data for Surface Boiling Liquids, Cambridge, Mass. M.I.T. Div. Ind. Cooporation. (1951). http://hdl.handle.net/1721.1/61431.

[25] K.G. Nayar, M.H. Sharqawy, L.D. Banchik, J.H. Lienhard, Thermophysical properties of seawater: A review and new correlations that include pressure dependence, Desalination. 390 (2016) 1–24. doi:10.1016/j.desal.2016.02.024.

[26] M.H. Sharqawy, J.H. Lienhard V, S.M. Zubair, Thermophysical properties of seawater: A review of existing correlations and data, Desalin. Water Treat. 29 (2011) 355–355. doi:10.5004/dwt.2011.2947.

[27] K.H. Chu, R. Enright, E.N. Wang, Structured surfaces for enhanced pool boiling heat transfer, Appl. Phys. Lett. 100 (2012). doi:10.1063/1.4724190.

Figures

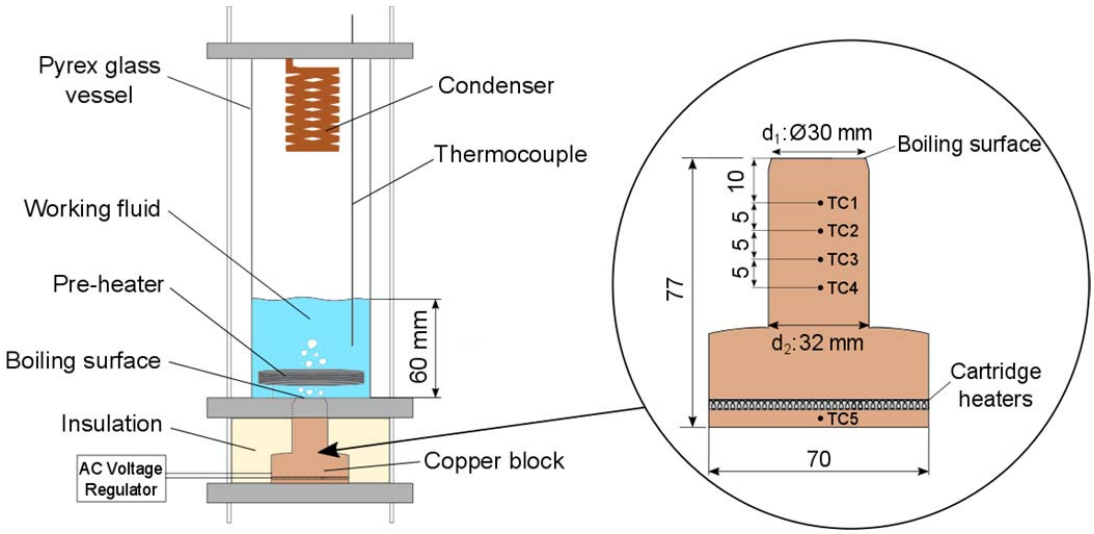

Figure 1 Schematic of the experimental apparatus and its main components. All dimensions are given in millimeters.

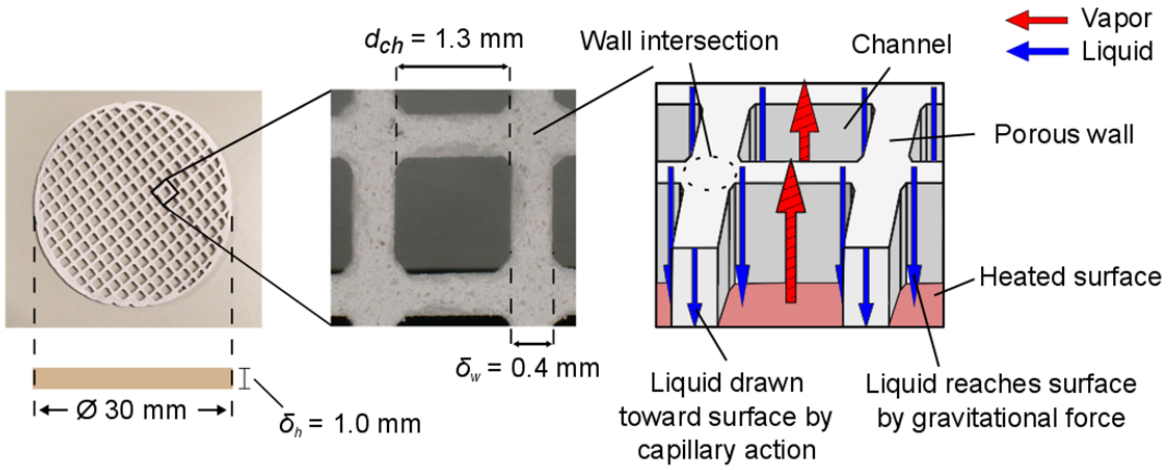

Figure 2 HPP used in this study and schematic of flow paths of liquid and vapor phases through the HPP.

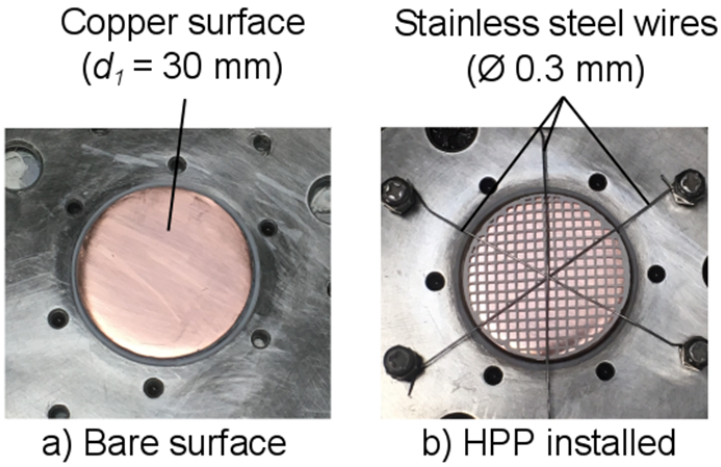

Figure 3 Images of (a) BS and (b) BS with HPP installed.

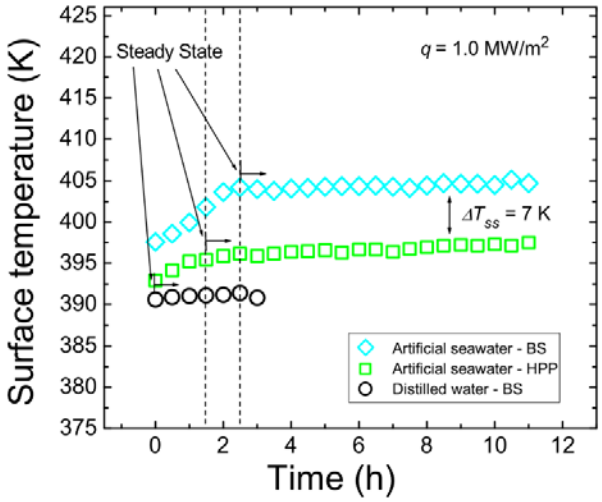

Figure 4 Temperature change in the surface for artificial seawater with and without HPP and distilled water without HPP under constant heat flux (1 MW/m^2).

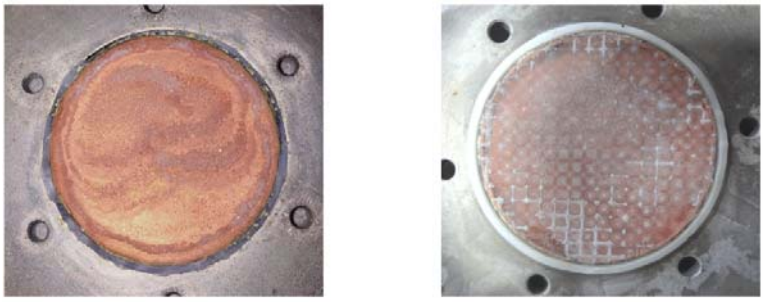

Figure 5 Images of salt deposition after artificial seawater pool boiling: (a) without and (b) with HPP.

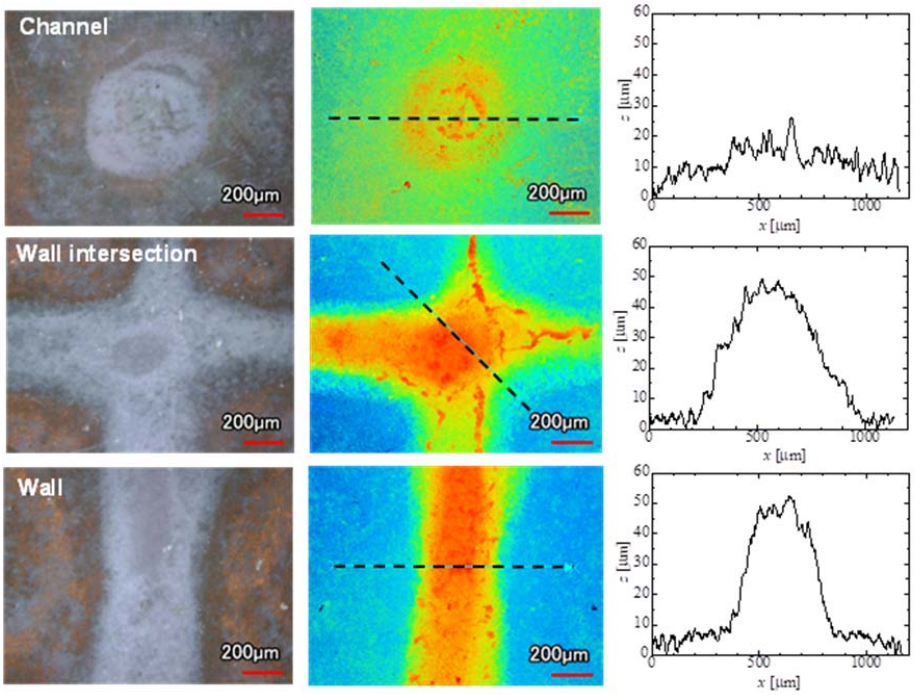

(a) Optical images (b) Height profile (c) Sectional view of the dashed line in (b)

Figure 6 Optical, height and 3D model images, obtained with the 3D Laser Scanning, from a channel, a wall intersection and wall position. The images show the pattern of the sea-salts deposits formed at these positions.

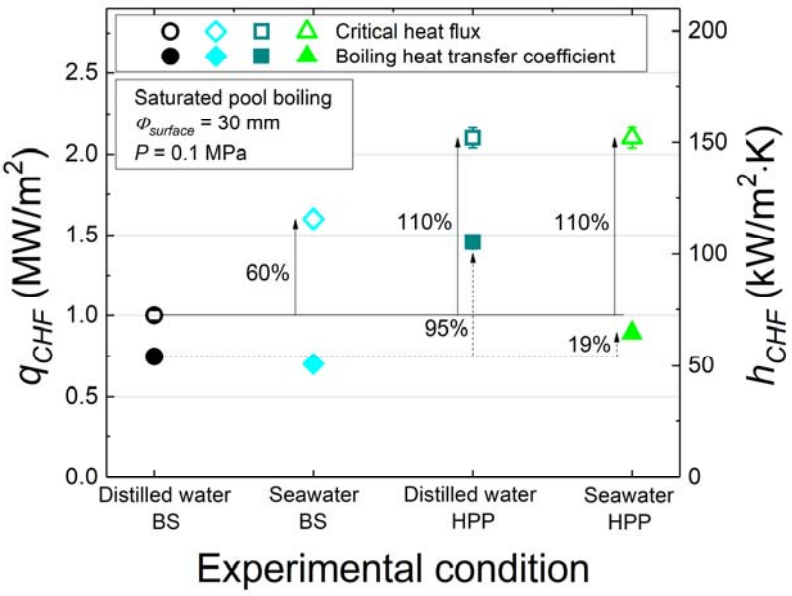

Figure 7 Results for CHF and BHTC from distilled water and seawater boiling with and without HPP. The percentages next to the arrows represent the enhancement relative to distilled water with BS.

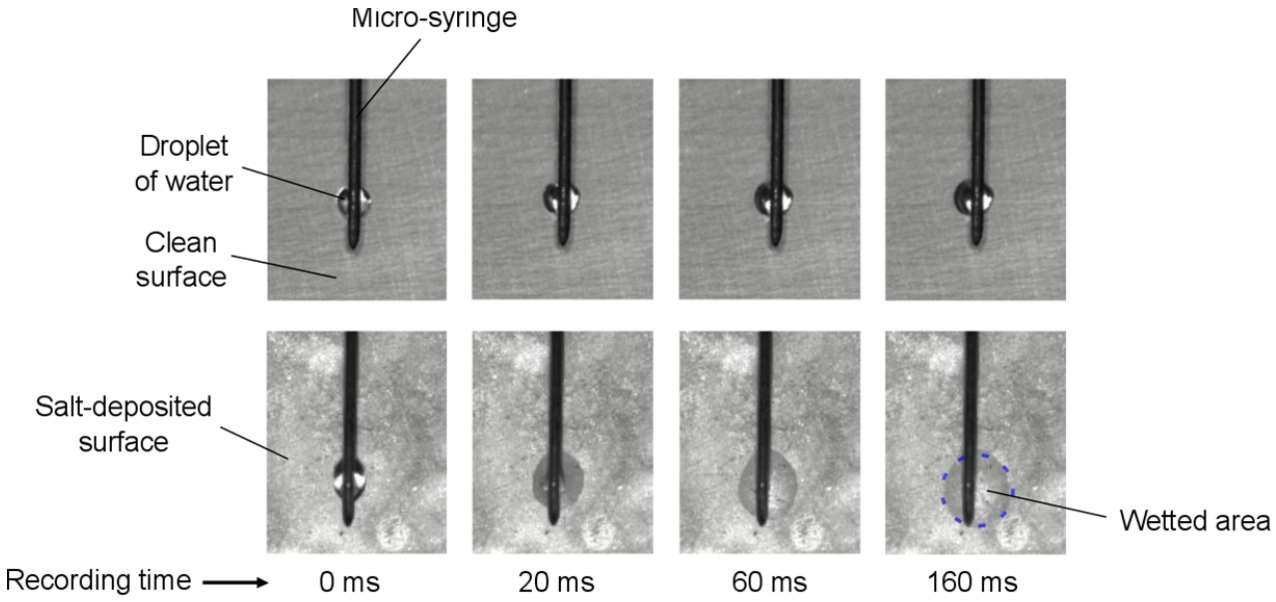

Figure 8 Wettability test on (upper) clean surface and (lower) salt-deposited surface.

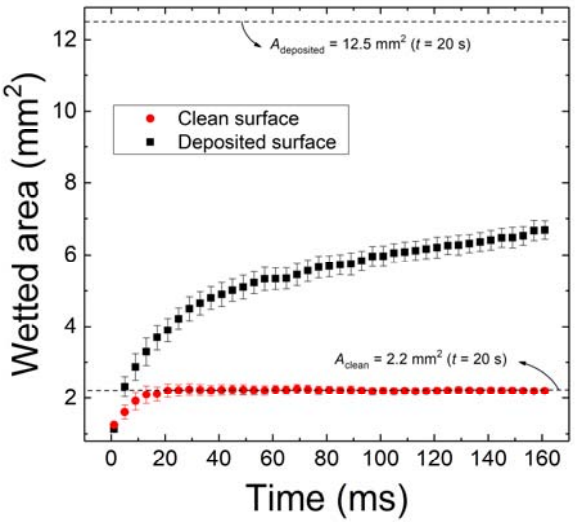

Figure 9 Wetted area as function of time on heating surface before and after artificial seawater pool boiling.

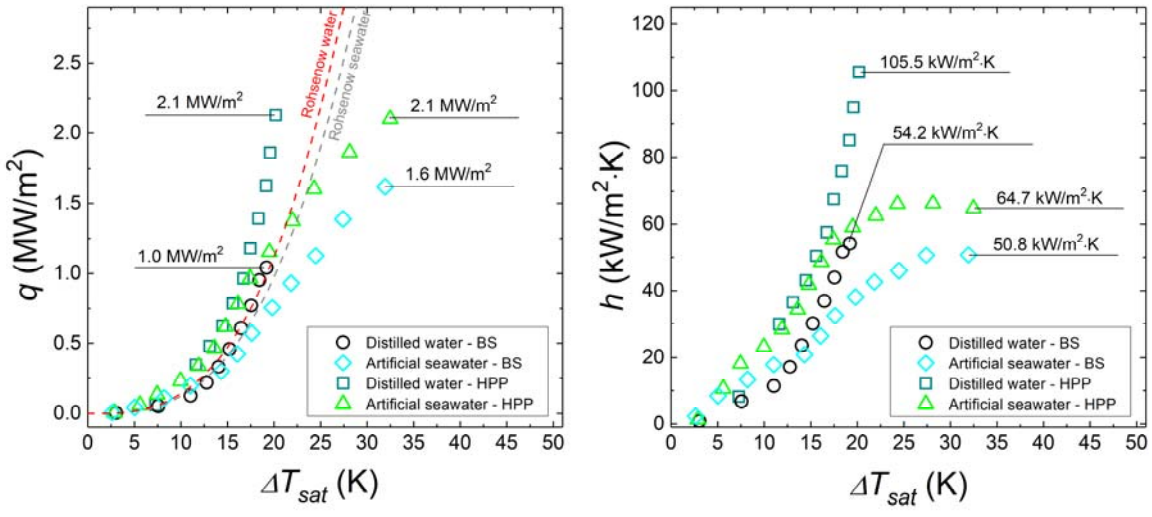

Figure 10 Boiling curves and BHTC of distilled water and artificial seawater with and without the HPP.

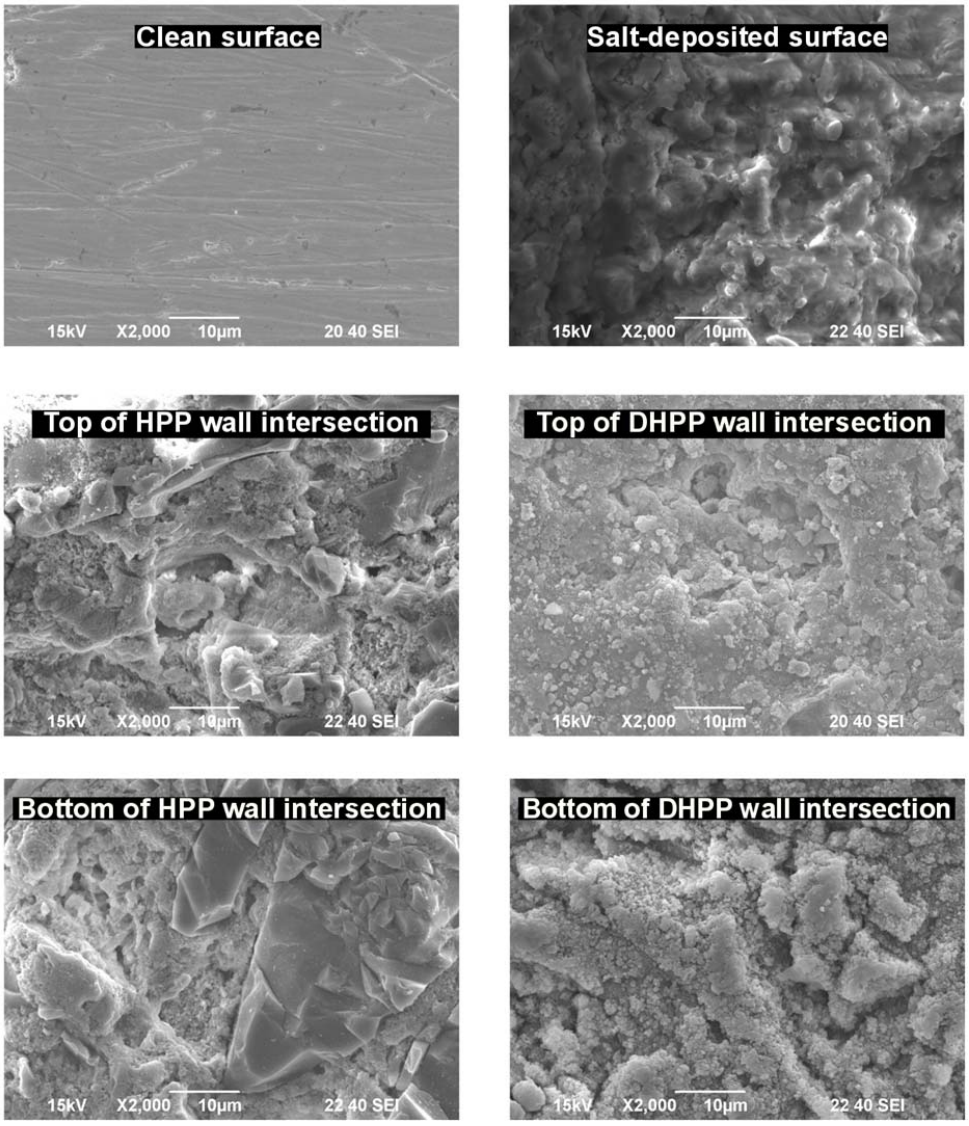

Figure 11 SEM images of copper and HPP surfaces (left) before and (right) after seawater pool boiling experiments.

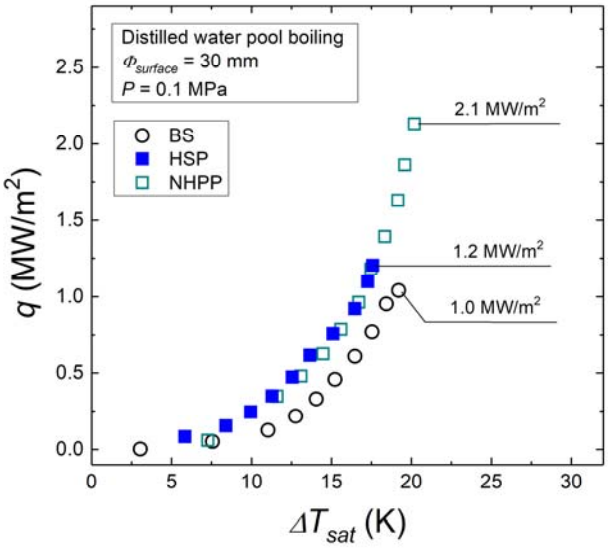

Figure 12 Boiling curves for distilled water on BS and with NHPP and HSP.

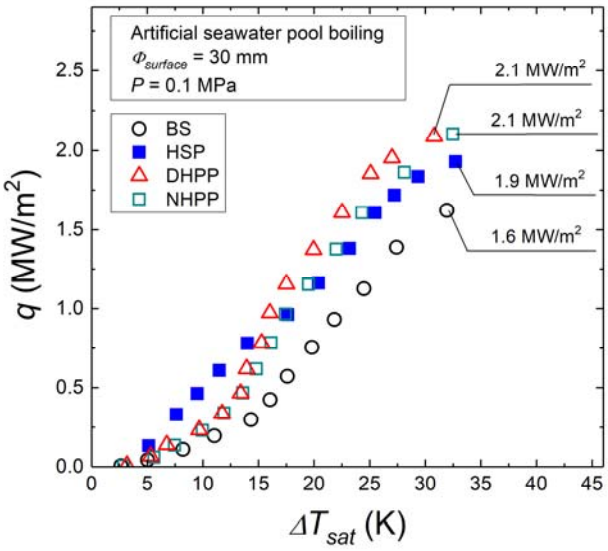

Figure 13 Boiling curves for artificial seawater on BS and with NHPP, DHPP, and HSP.

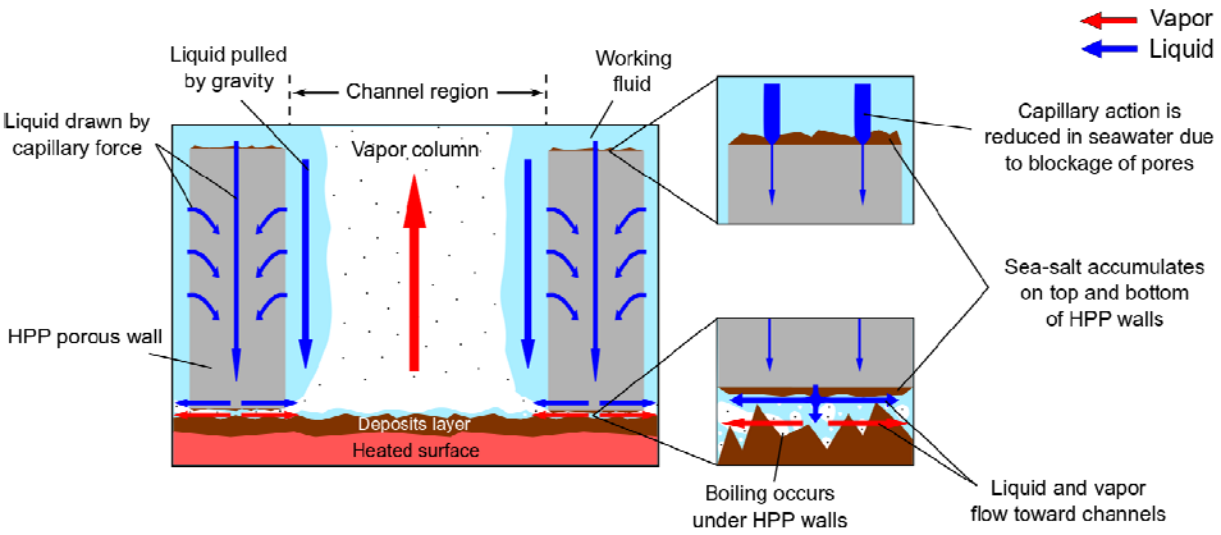

Figure 14 Sketch showing sea-salt deposition and liquid and vapor paths when HPP is installed.

Tables

Table 1 Main composition of artificial seawater and real seawater.

Element	Artificial seawater (g/L)	Representative seawater (g/L)*
Chlorine	20.60	19.35
Sodium	11.46	10.78
Magnesium	1.22	1.28
Sulfur	0.89	0.90
Calcium	0.41	0.41
Potassium	0.40	0.40
Strontium	0.01	0.01
Boron	0.002	0.004
Fluorine	0.001	0.001
Iodine	0.0001	0.0001

* Data for representative seawater composition from [20].

Table 2 Composition of sea-salts deposits.

Element	Atomic ratio (%)
Oxygen	42.5
Chlorine	21.2
Sodium	16.2
Magnesium	10.5
Carbon	6.4
Sulfur	1.4
Calcium	0.6
Potassium	0.5